

Displaced Neutrino Jets at the LHeC

Giovanna Cottin^{1,*}, Oliver Fischer^{2,†}, Sanjoy Mandal^{3,‡}, Manimala Mitra^{4,5,§} and Rojalin Padhan^{4,5,¶}

¹ *Departamento de Ciencias, Facultad de Artes Liberales,*

Universidad Adolfo Ibáñez, Diagonal Las Torres 2640, Santiago, Chile

² *Department of Mathematical Sciences, University of Liverpool, Liverpool, L69 7ZL, UK*

³ *AHEP Group, Institut de Física Corpuscular – CSIC/Universitat de València, Parc Científic de Paterna. C/ Catedrático José Beltrán, 2 E-46980 Paterna (Valencia) - SPAIN*

⁴ *Institute of Physics, Sachivalaya Marg, Bhubaneswar-751005, India and*

⁵ *Homi Bhabha National Institute, Training School Complex, Anushakti Nagar, Mumbai 400094, India*

(Dated: April 29, 2021)

Extending the Standard Model with right-handed neutrinos (RHNs) is well motivated by the observation of neutrino oscillations. In the type-I seesaw model, the RHNs interact with the SM particles via tiny mixings with the active neutrinos, which makes their discovery in the laboratory, and in particular at collider experiments in general challenging. In this work we instead consider an extension of the type-I seesaw model with the addition of a leptoquark (LQ), and employ a non-minimal production mechanism of the RHN via LQ decay, which is unsuppressed by neutrino mixing. We focus on relatively light RHN with mass $\mathcal{O}(10)$ GeV and LQ with mass 1.0 TeV, and explore the discovery prospect of the RHN at the proposed Large Hadron electron Collider. In the considered mass range and with the given interaction strength, the RHN is long lived and, due to it stemming from the LQ decay, it is also heavily boosted, resulting in collimated decay products. The unique signature under investigation is thus a displaced fat jet. We use kinematic variables to separate signal from background, and demonstrate that the ratio variables with respect to energy/number of displaced and prompt tracks are useful handles in the identification of displaced decays of the RHN. We also show that employing a positron beam provides order of magnitude enhancement in the detection prospect of this signature.

Introduction.— The observation of neutrino oscillations is a clear indicator for new physics beyond the Standard Model (BSM). A plethora of models exist that aim at explaining the light neutrino masses and mixings, many of which contain Standard Model (SM) gauge singlet right-handed neutrino (RHN). The simplest one among them is the type-I seesaw model [1], where the RHNs are Majorana particles. Being SM gauge singlet RHNs interact with the SM particles only via their mixing with the active neutrinos, referred to as active-sterile mixing, and is proportional to $\sqrt{\frac{m_\nu}{M_N}}$, where m_ν and M_N are the light neutrino and the RHN mass scale. Since $m_\nu < \text{eV}$, this mixing is small, leading to a suppressed production of RHN at colliders, which makes their observation challenging. This limitation can be avoided if RHNs are embedded in a theory framework with a new production mechanism that involves unsuppressed interactions of RHN with BSM/SM particles.

Motivated by this, we consider a theory framework that includes a \tilde{R}_2 leptoquark (LQ) and Majorana RHN. We con-

sider a mass of 1 TeV for LQ and focus on RHN with low mass $M_N \sim \mathcal{O}(10)$ GeV. The RHN in this framework interacts with the LQ and an up-type quark and can thus be produced from LQ decay. For the considered mass scales, the RHN is heavily boosted and its decay products leptons and jets are collimated, which fail to satisfy standard isolation criteria, thereby enabling a large radius jet description as the appropriate description to adopt. Additionally, a RHN in the considered mass range is a long lived particle and its decay is displaced from the point of its creation. The final state object of interest is thus a displaced large radius jet, or a fat jet, which is also accompanied by a prompt jet.

This signature is challenging to probe at the LHC due to its hadronic nature. Therefore, we investigate this signature in a relatively clean environment, *i.e.*, in lepton-hadron collisions at the proposed Large Hadron electron Collider (LHeC) [2]. The LHeC allows for resonant \tilde{R}_2 production with a sizeable cross-section, which has been shown to have a very good sensitivity to a LQ with first-generation coupling [3], cf also ref. [4, 5]. Moreover, the possibilities of electron polarisation and to use a positron beam provide extra handles to test the nature of the new physics signature [2, 5].

The paper is organized as follows: First we briefly review the model and the existing constraints on LQ. Following that we discuss the production of RHN at an ep collider LHeC. In the subsequent section, we present a detailed collider analy-

* giovanna.cottin@uai.cl

† oliver.fischer@liverpool.ac.uk

‡ smandal@ific.uv.es

§ manimala@iopb.res.in

¶ rojalin.p@iopb.res.in

sis and discuss discovery prospect of the unique RHN signature. Finally, we present the summary of the paper.

The Model.— We consider the \tilde{R}_2 leptoquark model, which contains a scalar LQ, and three RHN states (N_i). The LQ has two iso-spin components, $\tilde{R}_2(3, 2, 1/6) = (\tilde{R}_2^{\frac{2}{3}}, \tilde{R}_2^{-\frac{1}{3}})^T$, where the superscript of the components denotes the electromagnetic charge. The following renormalizable terms describe interactions of \tilde{R}_2 with the SM fermions and N_i [5, 7–10]:

$$\mathcal{L}_{LQ} = -Y_{ij}\bar{d}_R^i\tilde{R}_2^a\epsilon^{ab}L_L^{j,b} + Z_{ij}\bar{Q}_L^i\tilde{R}_2^a N_R^j + \text{H.c.} \quad (1)$$

In the above, $i, j = 1, 2, 3$ are flavor indices, $a, b = 1, 2$ are $SU(2)_L$ indices, and N_R indicates the right chiral component of N . Upon expansion, Eq. (1) becomes:

$$\begin{aligned} \mathcal{L}_{LQ} = & -Y_{ij}\bar{d}_R^i e_L^j \tilde{R}_2^{2/3} + (Y U_{PMNS})_{ij}\bar{d}_R^i \nu_L^j \tilde{R}_2^{-1/3} + \\ & Z_{ij}\bar{u}_L^i N_R^j \tilde{R}_2^{2/3} + (V_{CKM} Z)_{ij}\bar{d}_L^i N_R^j \tilde{R}_2^{-1/3} + \text{H.c.} \end{aligned} \quad (2)$$

Here, Y and Z are the 3×3 complex Yukawa coupling matrices, V_{CKM} and U_{PMNS} are the Cabibbo-Kobayashi-Maskawa and Pontecorvo-Maki-Nakagawa-Sakata matrices. To investigate the model signature, it is sufficient to assume that only one generation of RHN couples with leptons and quarks. We consider this to be N_1 (denoted henceforth as N), with only $Z_{11} \neq 0$, and all other Z_{ij} being 0. Additionally, we also consider only $Y_{11} \neq 0$. Due to the Y_{11}, Z_{11} couplings $\tilde{R}_2^{2/3}$ can decay to both ed and Nu states. We denote the corresponding branching ratios by β_{ed} and β_{Nu} , respectively.

Constraints.— Both direct and indirect experimental searches give strong constraints on a LQ state. Very relevant for LQ production at the LHeC is the precision measurement of atomic parity violation (APV), which tightly constrains the LQ coupling to a d quark and e state, as

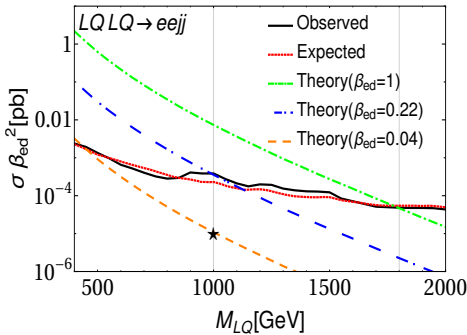


FIG. 1. Comparison between theory cross-section and the observed limit on $eejj$ cross-section from the LHC. The black line is the 13 TeV LHC limit on $\sigma\beta_{ed}^2$ [6]. The green, blue, orange lines represent the variation of theory cross-section $\sigma(pp \rightarrow LQLQ) \times \beta_{ed}^2$ w.r.t LQ mass. The star denotes our chosen benchmark couplings $Y_{11} = 0.2, Z_{11} = 1$, also consistent with the APV bound.

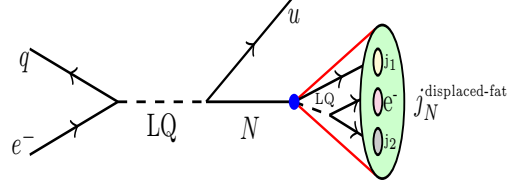


FIG. 2. Sample Feynman diagram for the model signature at the LHeC, the blue circle indicates displaced N decay.

$Y_{11} < 0.34 \frac{M_{LQ}}{1 \text{ TeV}}$ [11], M_{LQ} is the LQ mass. Evidently, for larger LQ mass the constraint on coupling Y_{11} relaxes. The tree level lepton flavour violating (LFV) Kaon decay $K_L \rightarrow \mu^- e^+$ also gives a tight constraint on the LQ couplings $|Y_{22} Y_{11}^*| \leq 2.1 \times 10^{-5} (\frac{M_{LQ}}{1 \text{ TeV}})^2$ [11, 12]. Due to our choice of $Y_{22} = 0$, this is not relevant for our study.

LHC search.— LQ are pair-produced in proton-proton collisions, which has been investigated in few different channels from the process $pp \rightarrow LQLQ \rightarrow \ell j \ell j$ [6, 13]. Non-observation of any signal at $\sqrt{s} = 13$ TeV constrains LQ masses to be larger than 1.8 TeV at 95% C.L [6] for LQ coupling exclusively to the first generation fermions. Including several decay channels simultaneously, in particular $LQ \rightarrow Nu$, relaxes the constraint on the LQ mass, as shown in Fig. 1. In the following we consider a large branching ratio $\beta_{Nu} = 96\%$ for $\tilde{R}_2 \rightarrow Nu$ production mode, which leaves a sufficiently small branching ratio β_{ed} for the $\tilde{R}_2 \rightarrow de$ decay to relax the LHC mass-limit to below 1 TeV. These branching ratios can be obtained for $Y_{11} = 0.2, Z_{11} = 1.0$. The point marked in star in Fig. 1 represents this benchmark.

It is important to realise that, as β_{ed} decreases, the branching ratio β_{Nu} becomes large, and $LQ \rightarrow Nu$ process could in principle be investigated at the LHC. We remind ourselves that the decay $\tilde{R}_2 \rightarrow Nu$ is followed by the decay of N leading to a displaced fat jet for $M_N = \mathcal{O}(10)$ GeV. We find that for our benchmark point the cross-sections for $pp \rightarrow LQLQ \rightarrow NuNu$, and $pp \rightarrow LQLQ \rightarrow edNu$ are $\sigma = 7.53, 0.31$ fb, respectively, which are much smaller than what we obtain from $ep \rightarrow Nu$ at LHeC, as discussed below. Additionally, the final state being all-hadronic and being hidden in the large QCD background at the LHC, we expect the sensitivity to be rather small. Hence for the study of the displaced fat jet, we rather choose to work with LHeC.

LQ decays.— For non-zero Y_{11}, Z_{11} couplings $\tilde{R}_2^{2/3}$ can decay to both ed and Nu states. The analytical expression for these two-body decays are,

$$\Gamma(LQ \rightarrow ed/Nu) = \frac{|Y_{11}|^2 f_1 / |Z_{11}|^2 f_2}{16\pi M_{LQ}^3}, \quad (3)$$

where $f_1 = \lambda^{\frac{1}{2}}(M_{LQ}^2, m_e^2, m_d^2)(M_{LQ}^2 - m_e^2 - m_d^2)$, $f_2 = \lambda^{\frac{1}{2}}(M_{LQ}^2, M_N^2, m_u^2)(M_{LQ}^2 - M_N^2 - m_u^2)$ and $\lambda(x, y, z) = x^2 + y^2 + z^2 - 2xy - 2xz - 2yz$. As shown by the green line in

Fig. 1, the LHC searches for the decay $LQ \rightarrow ed$ constrains LQ mass as $M_{LQ} > 1.80$ TeV, assuming a branching ratio $\beta_{ed} = 1$. Considering smaller branching fractions this lower bound relaxes to, for instance, $M_{LQ} = 1.0$ TeV when $\beta_{ed} = 0.22$. For $\beta_{ed} = 0.04$ the constraint is even more relaxed.

RHN decay.– For the chosen values of the couplings, the dominant decays of N are mediated via an off-shell \tilde{R}_2 . The contributions of SM mediators are suppressed by small active-sterile mixing. For the considered mass range N decays to $N \rightarrow e^- \bar{u}d, e^+ \bar{u}d$ via $\tilde{R}_2^{2/3}$ (two-body decays into lepton and pseudoscalar/vector meson are relevant for $M_N \leq \mathcal{O}(1)$ GeV). N can also decay to $N \rightarrow \nu q \bar{q}'$ via $\tilde{R}_2^{-1/3}$. The partial decay width for $N \rightarrow e^- \bar{u}d/e^+ \bar{u}d$ is:

$$\Gamma(N \rightarrow e^- \bar{u}d/e^+ \bar{u}d) = N_c \frac{|Z_{11}|^2 |Y_{11}|^2 M_N^5}{512\pi^3 M_{LQ}^4} \mathcal{I} \quad (4)$$

Here, $\mathcal{I} = I(x_u, x_d, x_e) = \int_{(x_d+x_e)^2}^{(1-x_u)^2} \frac{dz}{z} (1+x_u^2-z)(z-x_d^2-x_e^2)\lambda^{\frac{1}{2}}(1, x_u^2, z)\lambda^{\frac{1}{2}}(z, x_d^2, x_e^2)$ and $x_u/d/e = \frac{m_{u/d/e}}{M_N}$, and $N_c = 3$ is the color factor. $N \rightarrow \nu q \bar{q}'$ also has similar dependency on masses and couplings. The branching ratios for N decaying into $eq \bar{q}'$ and $\nu q \bar{q}'$ are 50% each. For $M_N < 50$ GeV, N has a proper decay length $c\tau_N > \mathcal{O}(1) \mu\text{m}$ for our chosen benchmark point. In particular for $M_N = 10$ GeV (20 GeV), $c\tau_N \sim 1$ mm ($c\tau_N \sim 0.01$ mm). On the other hand, for $M_N \geq 50$ GeV, $c\tau_N$ is less than $1 \mu\text{m}$, which is below the resolution of the LHeC and also LHC detectors, such that N decay cannot be considered as being displaced.

Signal.– Our stage is the LHeC with its 7 TeV proton and 60 GeV electron beam and without polarisation, where N is produced via $ep \rightarrow Nu$ process. The signal is dominated by resonant $\tilde{R}_2^{2/3}$ production with a cross section of 9.3 fb, followed by the subsequent decay $\tilde{R}_2^{2/3} \rightarrow Nu$ with 96% branching ratio, see Fig. 2 for sample diagram. This production channel strongly depends on the two couplings Y_{11} and Z_{11} . Also the t -channel contribution, mediated by $\tilde{R}_2^{2/3}$, contributes sizeably with $\sigma \sim 5.7$ fb. We remark, that the production of N via leptonic mixing is suppressed by mixing square $m_\nu/M_N < \mathcal{O}(10^{-10})$ and is therefore completely negligible in our model. The associated parton u hadronises and gives rise to a prompt light jet.

We consider both, e^- and e^+ in the initial state, which lead to different production cross sections [5] due to a difference in the quark PDFs. This could be a useful handle to fingerprint the signature, if it were to be observed. The production cross sections are shown in Fig. 3. The cross-sections are fairly large, $\sigma \sim 14, 127$ fb for e^- and e^+ beam, respectively, and increases even further if polarisation of e^-/e^+ beam is being used.

For the considered LQ mass $M_{LQ} = 1$ TeV, and N with mass $M_N \sim \mathcal{O}(10)$ GeV, N is produced with a boost and its proper decay length in the laboratory system is enhanced to

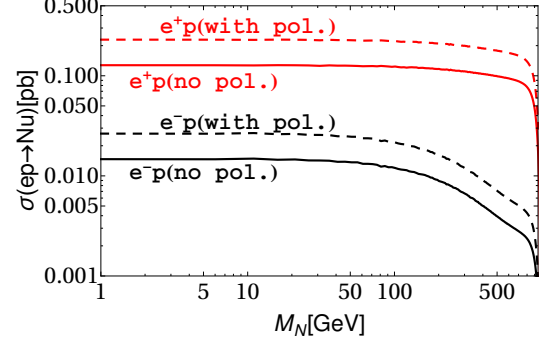


FIG. 3. Production cross-section of $ep \rightarrow Nu$ with and without 80% left (right) polarised e^- (e^+) beam.

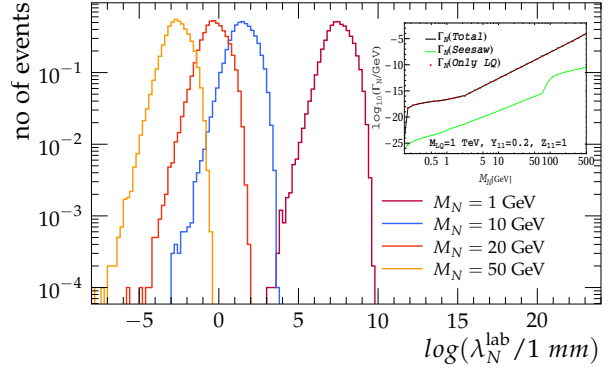


FIG. 4. Distribution of λ_N^{lab} , where the inset figure represents the proper decay width Γ_N of N . The green and red lines indicate contribution of (W, Z, h), and LQ states in three-body decay of N with the latter dominating Γ_N . For W, Z, h mediation, which depend on active-sterile mixing, we use $m_\nu = 0.1$ eV.

$\lambda_N^{\text{lab}} = \beta\gamma c\tau_N$, where $\beta\gamma = |p_N|/M_N > 1$ due to RHN momentum $p_N \sim M_{LQ}/2$. We show the distribution of λ_N^{lab} in Fig. 4. As can be seen, N with masses 10, 20 GeV undergoes displaced decays with decay length in the $\mathcal{O}(mm - 100mm)$ range, while for 50 GeV, this is almost a prompt decay.

The boost of N also leads to very small angular separation of its decay products, as shown in Fig. 5. Of particular interest is the separation between the charged lepton and the jets. As the figure shows, a sizeable fraction of the decays fails to satisfy the standard lepton isolation criterion, $\Delta R(\ell, j) > 0.4$ (ΔR between other decay products of N also display similar features), which is more pronounced for smaller M_N and implies that the leptons are not sufficiently isolated to be recognized as such. Instead, the N decay products tend to appear as a single jet with somewhat large radius, referred as a “fat jet”. Thus, the very specific signature under investigation is a fat jet that originates from a RHN displaced

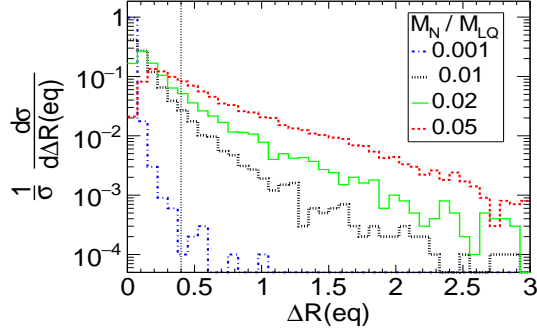


FIG. 5. $\Delta R(eq)$ separation of closely spaced lepton-quark pair. The vertical line is the typical isolation criterion.

vertex and is accompanied by a prompt jet:

$$e^\pm p \rightarrow jN \rightarrow j + j_N^{\text{displaced-fat}} \quad (5)$$

where $j_N^{\text{displaced-fat}}$ denotes the displaced and collimated decay products of the RHN, forming a fat jet, which we refer as a neutrino jet. Among the $N \rightarrow eq\bar{q}'$, $\nu q\bar{q}'$ decay modes, we focus on $N \rightarrow e^\pm q\bar{q}'$ and include these states in the fat jet description. In terms of sensitivity our results are thus conservative. The chosen decay mode has the added benefit that it allows the reconstruction of M_N . Additional channels $N \rightarrow \nu q\bar{q}'$ can be vetoed by imposing a missing transverse momentum cut. For a prompt fat jet signature in inverse seesaw model at LHeC, see [14].

Notice that, N is produced together with a prompt jet with substantial p_T and moderate η values. This jet emerges from the primary vertex and can be used to determine its three-coordinates. The corresponding uncertainty of this determination is related to the tracking precision, which is $\mathcal{O}(10) \mu\text{m}$ [4, 15]. In the subsequent discussion, while designing the cuts, we take for the transverse displacement a detection threshold of $50 \mu\text{m}$, to be conservative.

Backgrounds.— We consider a number of SM backgrounds, $ep \rightarrow ej, eb, \nu j, \nu jj, e bj, ebbb$, shown in Table. I. The relevant processes are those involving B -hadrons, which can give rise to displaced vertices. The light jet background is also important due to its huge cross-section, see Table. I. This is especially relevant for the heavier N which are quasi-prompt due to the short lifetime. The single top production $ep \rightarrow \nu \bar{t}$ is already included. Other background involving tau-lepton production $ep \rightarrow \nu j (W \rightarrow \nu \tau)$ ($\sigma_\tau = 0.01$ pb with our cuts) can be neglected. Our main focus is thus on the final states: $e/\nu + n_j j + n_b b$, with $n_j \geq 1$ and/or $n_b \geq 1$ being the number of light quarks and b quarks, respectively.

Simulation and event selection.— We use MadGraph5 aMC@NLO(v2.7) [16] to simulate both signal and background samples. For the generation of parton level signal events we implement the LQ model in FeynRules(v2.3) [17] and use the UFO files in MadGraph5 aMC@NLO(v2.7).

We implement the following generation level cuts for background event $p_T(b/j) > 20$ GeV, $p_T(\ell) > 10$ GeV, $|\eta(b/j/\ell)| < 5$, $\Delta R(jj/\ell j/bb/bj/lb) > 0.05$. We also demand transverse momentum p_T of leading parton > 150 GeV for background events, so that the majority of events populate the signal region. We use Herwig (7.2) [18, 19] to simulate the hadronization and showering of parton level events. For the signal, we consider the RHN decay in Herwig (7.2). We use Rivet (v3.0) [20, 21] for event analysis. For jet formation we use FastJet (v3.3.2) [22]. We reconstruct fat jet using a Cambridge-Aachen algorithm [23] with radius parameter $R = 1.0$. We select events according to the following criteria:

- $N_{jet} \geq 2$ and $p_T \geq 50$ GeV for all jets.
- We select all the charged final state particles (tracks) with $p_T > 1$ GeV in an event and calculate the transverse displacement $R_T = \sqrt{X^2 + Y^2}$ (X, Y being the coordinates of the production vertex) of each of the tracks from the interaction point (IP). The distribution is shown in the left panel of Fig. 6. For the signal the peaks occurring at a higher value of R_T are due to tracks originating from RHN decay. The high track multiplicity at a lower R_T is due to tracks associated with the prompt jet. For the light jet background (also for signal, and b jet background), peak at a higher R_T ($\simeq 200$ mm) occurs due to the presence of long-lived hadrons.
- We define the track as a displaced track if the transverse displacement is above the detection threshold, $R_T > 50 \mu\text{m}$. Subsequently, we define a ratio

$$r_N = \frac{N_{trk}(\text{displaced})}{N_{total-trk}}, \quad (6)$$

where $N_{trk}(\text{displaced})$ and $N_{total-trk}$ are the number of displaced tracks, and total number of tracks associated to a jet, respectively. Since N is long-lived this ratio is expected to be closer to 1 for jets originating from its decay vertex, while we expect a value $\ll 1$ for any other prompt jet. We also impose a bound $R_T < 312$ mm, so that we consider only those decay products appearing within the tracker volume. We label the jet having the largest value of r_N as the displaced jet. For N with $M_N \sim 50$ GeV the decays are rather prompt, and r_N can not be reliably used to identify the jet as stemming from N decay.

- We further cross-check if the displaced jet is originating from N and hence is a neutrino jet by computing the jet-mass. We identify a jet as the neutrino jet, if its invariant mass $M(j_N)$ is closest to M_N . We find that for $M_N \sim 10, 20$ GeV, the jet with highest r_N is consistent this invariant mass condition.

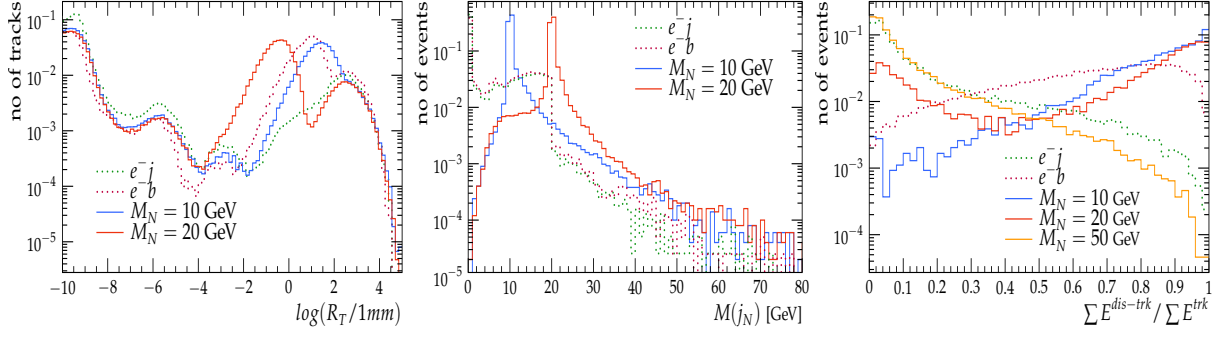


FIG. 6. Left panel: R_T distribution of the tracks. Middle panel: invariant mass distribution of neutrino jet. Right panel: distribution of the summed energy ratio of the displaced tracks and all possible tracks associated to the displaced jet.

Signal $ep \rightarrow j + j_N$	Background processes $e^-p/e^+p \rightarrow abc$									
	σ_b^i	ej	eb	νj	νjj	ebj	ejj	ebb	$e + 3j_b$	$\nu + 3j_b$
	6881.8 (5099.2)	89.9 (89.99)	9621.0 (3764.3)	3482.3 (1207.0)	20.08 (20.07)	2559.4 (1787.0)	32.67 (32.65)	1238.8 (890.5)	1394.3 (486.2)	
$M_N = 10$ GeV $\sigma_s^i = 7.37, \sigma_s^f = 3.5$ (e^-p) $\sigma_s^i = 64.03, \sigma_s^f = 42.97$ (e^+p)	σ_b^f	4.67 (3.46)	2.86 (2.87)	0 (0)	0.42 (0.14)	0.36 (0.37)	1.68 (1.18)	1.04 (1.04)	1.73 (1.25)	0.47 (0.16)
$M_N = 20$ GeV $\sigma_s^i = 7.21, \sigma_s^f = 3.37$ (e^-p) $\sigma_s^i = 63.92, \sigma_s^f = 44.65$ (e^+p)	σ_b^f	5.09 (3.77)	6.69 (6.69)	0 (0)	0.76 (0.26)	1.01 (1.03)	2.51 (1.75)	2.48 (2.48)	3.24 (2.33)	0.72 (0.25)
$M_N = 30$ GeV $\sigma_s^i = 7.1, \sigma_s^f = 1.59$ (e^-p) $\sigma_s^i = 63.7, \sigma_s^f = 25.09$ (e^+p)	σ_b^f	1.65 (1.22)	2.83 (2.84)	0.19 (0.07)	0.42 (0.14)	0.64 (0.65)	1.64 (1.14)	1.14 (1.14)	2.0 (1.44)	0.69 (0.24)

TABLE I. Initial and after cut cross-sections (in fb) for signal and backgrounds, which are denoted as $\sigma_s^{i,f}$ and $\sigma_b^{i,f}$ respectively. For background processes j_b implies including light jet and b jet. The numbers without (within) brackets are for e^- (e^+) mode, respectively.

- We define a variable r_E as the ratio of the sum of energies of the displaced tracks and sum of energies carried out by all tracks associated to a jet:

$$r_E = \frac{\Sigma E(\text{displaced} - \text{trk})}{\Sigma E(\text{trk})}, \quad (7)$$

We show the distribution of this variable in Fig. 6 for the jet with highest r_N . As can be seen, the distribution for displaced signal and light jet background are complementary in nature, which is instrumental in separating the two. For small N masses majority of the tracks are displaced, leading to a higher energy ratio r_E . For light jet background, reverse is true.

- Finally we select those events where the neutrino jet satisfies the following cuts: $r_N \geq 0.5$, $r_E \geq 0.5$, $p_T(j_N) \geq 150$ GeV and $M(j_N) = M_N \pm 3$.

Results.- The signal cross-sections for 10-30 GeV M_N varies as $\sigma_s^i \sim 7.10 - 7.37$ fb before applying any cut for

M_N [GeV]	n_σ	\mathcal{L} [fb^{-1}]	\mathcal{Y}^{ex}
10	6.0 (41.5)	34.0 (0.7)	0.067 (0.035)
20	4.7 (39.7)	56.8 (0.8)	0.059 (0.017)
30	3.3 (30.4)	116.6 (1.3)	0.047 (0.013)

TABLE II. n_σ is the significance of the proposed signature with only 50 fb^{-1} luminosity. \mathcal{L} is the required luminosity to achieve 5σ significance. Numbers without (within) brackets corresponds to e^- (e^+) beam, respectively. \mathcal{Y}^{ex} represents 2σ exclusion on Y_{11} .

e^- mode (see Table. I). The final cross-sections after all the cuts are $\sigma_s^f \sim 1.6 - 3.5$ fb. For $M_N = 50$ GeV as the decay is almost a prompt decay, we do not include the result in the table. We find the backgrounds eb, ej are the most relevant ones after cuts, while other backgrounds $ebb/ebbb, ejj/ejjj$ also give sizeable contributions. Applying a veto on missing transverse momentum will further suppress the $\nu j/\nu jj/\nu + 3j_b$ backgrounds. Instead, here we present a conservative

estimate. For the e^+ mode, the signal cross-section is one order of magnitude larger as compared to e^- mode, while the backgrounds are relatively smaller. The signal sensitivity is calculated as

$$n_\sigma = \sqrt{\mathcal{L}} \frac{\sigma_s^f}{\sqrt{\sigma_s^f + \sigma_b^f}} \quad (8)$$

where \mathcal{L} in fb^{-1} is the required luminosity to achieve n_σ significance, σ_s^f/σ_b^f are the after-cut signal/background cross sections. Our findings are summarised in Table II.

For the considered RHN masses, our signature can be detected with 5σ significance with an integrated luminosity $\mathcal{L} < 120 \text{ fb}^{-1}$. With the total integrated luminosity of 1000 fb^{-1} in the e^- mode, excluding our signal at 2σ significance can be used to put an upper limit on Yukawa $Y_{11} \leq 0.067$ for $M_N = 10 \text{ GeV}$. For higher RHN mass $M_N = 30 \text{ GeV}$, the limit becomes stringent due to the increase in geometric cut-efficiency ($R_T < 312 \text{ mm}$).

The table further shows that the e^+ mode clearly outperforms the e^- mode as signal sensitivity n_σ increases by almost one order of magnitude, and 5σ significance can be achieved with luminosities $\mathcal{L} < 2 \text{ fb}^{-1}$ only, for all the mass points considered. With $\mathcal{L} = 1000 \text{ fb}^{-1}$ the upper limit on Yukawa tightens $Y_{11} \leq 0.013$ for $M_N = 30 \text{ GeV}$. The signal sensitivity can be further improved with polarised e^- and e^+ beams due to increase in signal cross-section.

Conclusions.— In this article we considered a model that includes an \tilde{R}_2 LQ with $M_{LQ} = 1 \text{ TeV}$ and RHN with a mass of $\mathcal{O}(10) \text{ GeV}$. The RHN can be produced from resonant LQ decay, with comparatively large cross sections, and also via t channel processes. We studied the prospects of discovering the RHN at the LHeC via a displaced fat jet signature, which is purely hadronic in nature and therefore difficult to detect at the LHC. We perform a detailed analysis of the signal and the different SM background processes. We find that the ratio of energy deposits of the displaced and all possible tracks associated with the displaced jet is instrumental in separating displaced decays of RHN from background. We find that RHN in the considered mass range can be detected at the LHeC with only $\mathcal{L} < 120$ (2) fb^{-1} luminosity with $e^-(e^+)$ beam. We observe that, the use of a positron beam at LHeC clearly enhances the detection prospect of this signature by order of magnitude.

Acknowledgements

G.C. acknowledges support from ANID FONDECYT-Chile grant No. 3190051. The work of S.M. is supported by the Spanish grant FPA2017-85216-P (AEI/FEDER, UE), PROMETEO/2018/165 (Generalitat Valenciana). M.M thanks Indo-French Centre for the Promotion of Advanced Research for the funding (project no: 6304-2).

-
- [1] P. Minkowski, *Phys. Lett. B* **67**, 421 (1977).
[2] J. Abelleira Fernandez *et al.* (LHeC Study Group), *J. Phys. G* **39**, 075001 (2012), arXiv:1206.2913 [physics.acc-ph].
[3] J. Zhang, C.-X. Yue, and Z.-C. Liu, *Mod. Phys. Lett. A* **33**, 1850039 (2018).
[4] P. Agostini *et al.* (LHeC, FCC-he Study Group), (2020), arXiv:2007.14491 [hep-ex].
[5] R. Padhan, S. Mandal, M. Mitra, and N. Sinha, *Phys. Rev. D* **101**, 075037 (2020), arXiv:1912.07236 [hep-ph].
[6] G. Aad *et al.* (ATLAS), *JHEP* **10**, 112 (2020), arXiv:2006.05872 [hep-ex].
[7] I. Doršner, S. Fajfer, A. Greljo, J. Kamenik, and N. Košnik, *Phys. Rept.* **641**, 1 (2016), arXiv:1603.04993 [hep-ph].
[8] W. Buchmuller, R. Ruckl, and D. Wyler, *Phys. Lett. B* **191**, 442 (1987), [Erratum: *Phys.Lett.B* 448, 320–320 (1999)].
[9] W. Buchmuller and D. Wyler, *Phys. Lett. B* **177**, 377 (1986).
[10] S. Mandal, M. Mitra, and N. Sinha, *Phys. Rev. D* **98**, 095004 (2018), arXiv:1807.06455 [hep-ph].
[11] I. Dorsner, S. Fajfer, and A. Greljo, *JHEP* **10**, 154 (2014), arXiv:1406.4831 [hep-ph].
[12] I. Dorsner, J. Drobnak, S. Fajfer, J. F. Kamenik, and N. Kosnik, *JHEP* **11**, 002 (2011), arXiv:1107.5393 [hep-ph].
[13] A. M. Sirunyan *et al.* (CMS), *Phys. Rev. D* **99**, 052002 (2019).
[14] A. Das, S. Jana, S. Mandal, and S. Nandi, *Phys. Rev. D* **99**, 055030 (2019), arXiv:1811.04291 [hep-ph].
[15] K. Cheung, O. Fischer, Z. S. Wang, and J. Zurita, (2020), arXiv:2008.09614 [hep-ph].
[16] J. Alwall, R. Frederix, S. Frixione, V. Hirschi, F. Maltoni, O. Mattelaer, H. S. Shao, T. Stelzer, P. Torrielli, and M. Zaro, *JHEP* **07**, 079 (2014), arXiv:1405.0301 [hep-ph].
[17] A. Alloul, N. D. Christensen, C. Degrande, C. Duhr, and B. Fuks, *Comput. Phys. Commun.* **185**, 2250 (2014), arXiv:1310.1921 [hep-ph].
[18] J. Bellm *et al.*, *Eur. Phys. J. C* **76**, 196 (2016), arXiv:1512.01178 [hep-ph].
[19] M. Bahr *et al.*, *Eur. Phys. J. C* **58**, 639 (2008), arXiv:0803.0883 [hep-ph].
[20] C. Bierlich *et al.*, *SciPost Phys.* **8**, 026 (2020), arXiv:1912.05451 [hep-ph].
[21] A. Buckley, J. Butterworth, L. Lonnblad, D. Grellscheid, H. Hoeth, J. Monk, H. Schulz, and F. Siegert, *Comput. Phys. Commun.* **184**, 2803 (2013), arXiv:1003.0694 [hep-ph].
[22] M. Cacciari, G. P. Salam, and G. Soyez, *Eur. Phys. J. C* **72**, 1896 (2012), arXiv:1111.6097 [hep-ph].
[23] Y. L. Dokshitzer, G. D. Leder, S. Moretti, and B. R. Webber, *JHEP* **08**, 001 (1997), arXiv:hep-ph/9707323.